Revista EIA

UNIVERSIDAD EIA

Synthesis and characterization of $Eu_3Ba_5Cu_8O_{18-\delta}$ superconductor doped with 0.1% Graphene oxide

Revista EIA
ISSN 1794-1237
e-ISSN 2463-0950
Año XIX/ Volumen 21/ Edición N.42
Julio - diciembre de 2024
Reia4201 pp. 1-20

Publicación científica semestral
Universidad EIA, Envigado, Colombia

Para citar este artículo / To reference this article /
Segura Peña S.; Parra Suárez L.F.; Maldonado Cárdenas M.R.; Segura-Peña J. D.; Ayala Sotelo L. Synthesis and characterization of $Eu_3Ba_5Cu_8O_{18-\delta}$ superconductor doped with 0.1% Graphene oxide Revista EIA, 21(42), Reia4201. pp. 1-20. https://doi.org/10.24050/reia.v21i42.1785

Autor de correspondencia:

Segura Peña S.
Universidad Santo Tomás, Colombia.
sully.segura01@usantoto.edu.co

Recibido: 02-10-2023
Aceptado: 27-05-2024
Disponible online: 01-07-2024

Segura Peña S.[1,2]
Parra Suárez L.F[1]
Maldonado Cárdenas M.R[1]
Segura-Peña J. D[1]
Ayala Sotelo L.[1]

1. Universidad Santo Tomás, Colombia.
2. Universidad de Oviedo. Asturias, España.

Abstract

This research presents the synthesis and evaluation of the structural and morphological properties of superconducting $Eu_3Ba_5Cu_8O_{18-\delta}$ doped with 0.1% graphene oxide, using the solid state reaction method. The structural analysis performed on the samples, both doped and undoped, allowed identifying the main phase as $Eu_3Ba_5Cu_8O_{18-\delta}$ (Eu358), with orthorhombic structure and space group *Pmm2(25),* maintaining superconducting properties in both cases. In addition, it was observed that doping with graphene oxide resulted in the formation of a minority phase of $EuBa_4Cu_3O_9$ (Eu143), with cubic structure and space group *P23(195).* As for the morphological characterization, it was evidenced that the undoped sample presents aggregates formed by non-uniform size grains, with an average size of approximately 97 µm. In contrast, the sample doped with 0.1% graphene oxide exhibits significant improvements in uniformity and grain boundaries, with an average size of about 141 µm. These results confirm obtaining $Eu_3Ba_5Cu_8O_{18-\delta}$ with a 73% superconducting phase, exceeding the percentages previously reported using the solid-state reaction method.

Keywords: superconductor; (re)bco; graphene oxide; solid state reaction; rietveld refinement.

Síntesis y caracterización del superconductor $Eu_3Ba_5Cu_8O1_{8-\delta}$ dopado con 0.1% de óxido de Grafeno

Resumen

Esta investigación presenta la síntesis y evaluación de las propiedades estructurales y morfológicas del superconductor $Eu_3Ba_5Cu_8O_{18-\delta}$ dopado con un 0.1% de óxido de grafeno, utilizando el método de reacción de estado sólido. El análisis estructural realizado en las muestras, tanto en la no dopada como en la dopada, permitió identificar la fase principal como $Eu_3Ba_5Cu_8O_{18-\delta}$ (Eu358), con estructura ortorrómbica y grupo espacial *Pmm2*(25), manteniendo propiedades superconductoras en ambos casos. Además, se observó que el dopaje con óxido de grafeno dio lugar a la formación de una fase minoritaria de $EuBa_4Cu_3O_9$ (Eu143), con estructura cúbica y grupo espacial *P23*(195). En cuanto a la caracterización morfológica, se evidenció que la muestra no dopada presenta agregados conformados por granos de tamaño no uniforme, con un tamaño medio con un tamaño medio de aproximadamente 97 µm. En contraste, la muestra dopada con un 0.1% de óxido de grafeno exhibe mejoras significativas en la uniformidad y límites de los granos, con un tamaño medio de alrededor de 141 µm. Estos resultados confirman la obtención de $Eu_3Ba_5Cu_8O_{18-\delta}$ con una fase superconductora del 73%, superando los porcentajes reportados previamente utilizando el método de reacción de estado sólido.

Palabras claves: superconductor; (re)bco; oxido de grafeno; reacción de estado sólido; refinamiento rietveld.

1. Introduction

Study of high-temperature superconductor materials (HTSCs) has aroused a growing interest since its discovery in 1986, (JG, 1986) due to its broad spectrum of applications in science and technology field. (Delamare et al., 2000); Rekaby et al., 2014). During the last three decades, studies have been realized on the system YBaCuO-YBCO, which have demonstrated to be a superconductor material, composed by yttrium, barium and copper oxides. (Hor et al.,1987) Among the various kinds of high-temperature superconductors, $Y_3Ba_5Cu_8O_{18-\delta}$ (Y358) is a remarkable system, with a critical temperature Tc ≥ 100 K, which crystallizes in an orthorhombic structure assembled by five CuO_2 planes and three CuO chains. (Tavana et al.,2010). The number of planes and chains contributes to a higher conductivity (Suan et

Revista EIA https://doi.org/10.24050/reia.v21i42.1785

al., 2012) and, as a result, to various physical properties and critical temperatures. (Aliabadi et al., 2009). Due to the increment of its Tc, there has been a lot of interest among the scientific comunity, since it opens the door to many technological applications, like the creations of superconductor magnets, magnetic nuclear resonance, highly efficient electric motors, transport systems based on electric energy, particle accelerators and magnetic levitation trains, among others. (Aliabadi et al.,2009, Shoushtari et al., 2018).

Research efforts have been oriented towards substituting ytrium cation (Y) for rare-earth elements (RE) such as: La, Pr, Nd, Sm, Eu, Gd, Dy, Ho and Yb, with the aim of improving physical properties and critical parameters for the superconductors. (Alviz et al.,2017, Supelano et al., 2014). Specially, Europium (Eu) is notable for its partially full and highly localized orbitals, which can coexist with superconductivity. (Debessai et al., 2010). The results obtained with the inclusion of RE elements, revealed an increase in lattice parameters *a* and *c*, and also for the unitary cell volume as the atomic radius increases. Ionic radius for the RE atoms contributes significantly to Tc, since Tc tends to augment as the ionic radius for RE elements grow close to yttrium's radius size. (Parra et at., 2021) RE-358 compound has shown to be efficient for improving flux fixation capacity and inter-granular and superconductive properties. This system presents a dense microstructure with low porosity, and particle size tends to increase with ionic radius and sintering temperature. (Gaona et al., 2020).

On a different note, graphene based chemical doping has been used on HTSCs materials, in order to optimize its properties. (Falahati et al.,2019, Wei, et al., 2018) Graphene oxide (OG) is a material that highlights for its mechanical, optical and electronic properties, along with a good thermal and electric conductivity. (Dadras et al., 2018, Sahoo, et al., 2020). It is composed by carbon and oxygen atoms; the presence of oxygen atoms gives OG mechanical stability and makes it chemically active, highly used in several electronic and optoelectronic applications, as well as energy storage and conversion. (Zhu et al., 2010). Previous works have shown that lattice tension augments with OG doping for YBCO, the OG does not enter into the structure but

stays among the grains and performs a weak-bond role between the superconductive material grains. (Dadras et al 2018).

Besides, Dadras et al, (Dadras et al 2018).indicate that OG adding at 0.7 % in weight does not affect the crystalline structure, but improve critical parameters and grain connections for OG doped samples. Sahoo et al, (Sahoo et al, 2019). Reported that adding of graphene nanoplatelets to YBCO superconductor improves said superconductor parameters without affecting structural parameters, increases grain connectivity through weak bond mechanism, thus reducing irregularities, holes and material pores, hence augmenting critical current density for the material. Likewise, Kumar et al. (Kumar et al., 2013). studied OG doping effects on structural and superconductive properties for MgB_2. Their findings show that doped MgB_2 samples have a higher value for critical current density, superior critical magnetic field, and irreversibility field, as compared with non-doped samples. Consequently, the present work will be centered around $Y_3Ba_5Cu_8O_{18-\delta,}$ superconductor where Y cation is replaced by Europium (Eu), thus generating the system $Eu_3Ba_5Cu_8O_{18-\delta}$ abbreviated as Eu358. Synthesis is realized through solid state reaction method, and a 0.1% OG doping is applied. So far, there has not been found any inform studying the effects of OG doping on Eu358. Also, structural properties will be evaluated by X-Rays diffraction (DRX) as well as Rietveld refinement, and morphological analysis mediated by scanning electron microscopy (SEM).

2. Experimental

Eu358 system was prepared by the conventional solid state reaction method (RES). For the sintering process, the following stoichiometric quantities for oxides were used: Eu_2O_3 (99.99%), BaO (99.99%) and CuO (99.99%). These oxides were mixed and macerated for 4 hours. Then, they were compacted with a 5MPa pressure, and were calcined at 850°C for a period of 34 hours. Synthesis phase was performed at 950°C during 34 additional hours. Once these stations were completed, an oxygen flux of 100mL/min was introduced, followed

Revista EIA https://doi.org/10.24050/reia.v21i42.1785

by a gradual cooling down to 300°C, a process that extended 9 hours until reaching room temperature.

Structural properties of the calcined solids were analyzed through X-Ray Diffraction method (DRX) using a PANalytical X'Pert PRO-MPD diffractometer, equipped with ultra rapid X'celerator detector and a Bragg-Brentano configuration. Cu Kα (λ = 1.54186 Å) radiation in the range 20 and 90° was employed. Each measurement was performed with a 40 KV voltage and a 20mA current. For Rietveld refinement of diffraction pattern, GSAS (Toby 2001) and PCW (Kraus et al.,1996)) programs were used. The morphological features were studied through scanning electron microscopy (SEM) with a JEOL apparatus, and model JSM 6490-LV. Micrography analysis was performed with the program ImageJ. (Schneider et al., 2012) For sample composition, dispersive energy X-ray spectra (EDX) by using an X-ray canon coupled to the scanning electron microscope.

3. Results and Discussion

3.1 Structural analysis

Fig. 1a presents a difractogram for $Eu_3Ba_5Cu_8O_{18-\delta}$, synthesized sample, noting a hit degree of crystallinity with well defined signals. Phase identification was done by using X'Pert® High Score software, and the 2004 PDF-2 database, and comparing the results with previous research. (Landínez et al., 2012, Guerrero et al., 2021). This analysis allowed identification of three crystalline phases: main phase, $EuBa_5Cu_8O_{18-\delta}$ (Eu358), crystalized in an orthorhombic structure with space group *Pmm2* (25) and characterized by being superconductor. Secondary phases include $EuBa_2Cu_3O_{6.4}$ (Eu123), that shows a tetragonal crystalline structure (non-superconductor), with space group *P4/mmm* (123), and $BaCuO_2$, which exhibits a cubic crystalline structure with space group *Im-3m* (229).

Figura 1. XRD pattern of the a) Eu3Ba5Cu8O18-δ un doped, b) Eu3Ba5Cu8O18-δ with 0.1% of graphene oxide obtained by solid-state reaction.

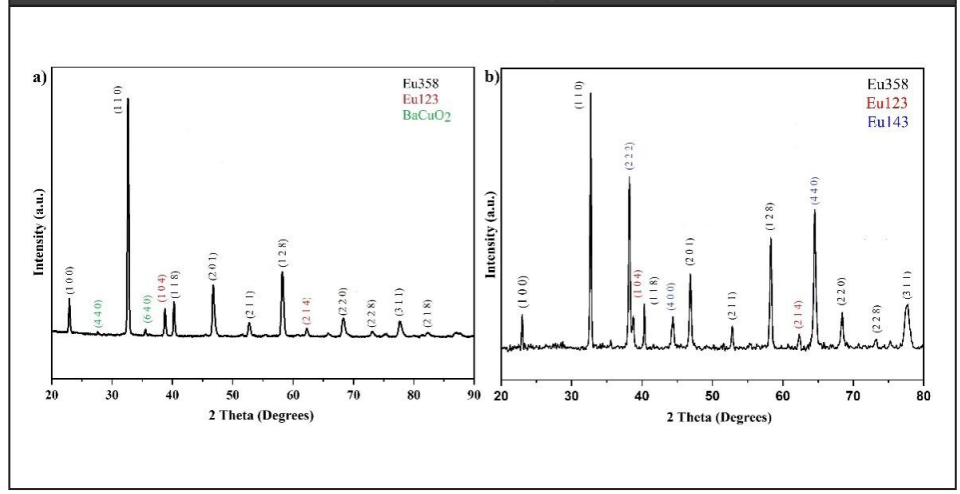

Fig. 1b, shows $Eu_3Ba_5Cu_8O_{18-\delta}$ difractogram with 0.1% OG. The analysis revealed a main phase $EuBa_5Cu_8O_{18-\delta}$ (Eu358), with orthorhombic structure and space group *Pmm2* (25). As a secondary phase, $EuBa_4Cu_3O_9$ (Eu143) was identified with a cubic structure and space group *P23* (195), while as a minority phase $EuBa_2Cu_3O_{6.4}$ (Eu123) was found, with tetragonal crystalline structure and space group *P4/mmm* (123). The presence of Eu143 phase was previously informed in materials superconductors (Gadzhimagomedov et al., 2021).

However, since thermal treatments were equal during synthesis for both samples, this phase presence can be attributed to OG, which diminished diffusion processes and originated the formation of majority phase Eu143, thus for bidding the orthorhombic phase Eu358 from appearing. Besides, the difractogram does not show OG presence, due to the low percentage in which the sample was found (0.1%), which is a hindrance in detecting any OG with X-rays diffraction technique. Starting from the obtained difractograms, the crystal size was determined with help of Scherrer's equation:

$$\beta_{hkl} = \frac{K\lambda}{FWHM cos\theta} (1)$$

Revista EIA https://doi.org/10.24050/reia.v21i42.1785

Where β_{hkl} represents crystal size; *K* is a non-dimensional form factor (typical value 0.9); λ is the X rays wavelength (λ=1.54056 Å);*FWHM* is the full width at half maximum for the most intense signal in the difractogram, with orientation (1 1 0) and θ is Bragg's angle. This lead us to crystal size calculation of 35.9 nm for the Eu358 sample and 43.4 nm for the Eu358 with 0.1% OG. In realizing a comparative analysis (see Fig. 2), it is observed that the sample contains a lesser proportion of secondary phases and the one with highest crystallinity is $EuBa_5Cu_8O_{18-\delta}$, which is the reason it was selected for Rietveld refinement through GSAS software, as shown in Fig. 3. For this figure experimental data is denoted with "x", the red line corresponds to the refined theoretical model, a green line corresponds to the background and the blue one is the difference between the experimental and theoretical difractograms.

Figura 2. Comparative diffractogram of the XRD pattern of the a) $Eu_3Ba_5Cu_8O_{18-\delta}$ undoped b) $Eu_3Ba_5Cu_8O_{18-\delta}$ with 0.1% of graphene oxide obtained by solid-state reaction.

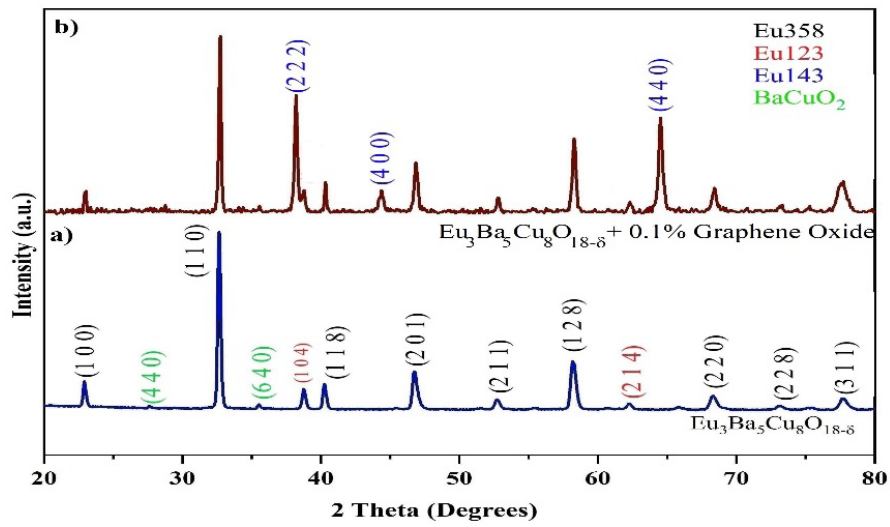

Cell parameters obtained by refinement are shown in Table 1, where it is evident the majority formation of Eu358 superconductor phase with 73.08% percentage, which surpasses the 34.96% purity obtained by other authors using the same method (Gaona et al.,

2020, Gadzhimagomedov et al., 2021). These achievements are associated to the molturation process performed as well as the 950°C temperature which favored the diffusion process and the formation of the desired crystal phase. These results are a significant contribution in the superconductor synthesis field.

Figura 3. Refined XRD patterns for the $Eu_3Ba_5Cu_8O_{18-\delta}$ undoped obtained by solid-state reaction.

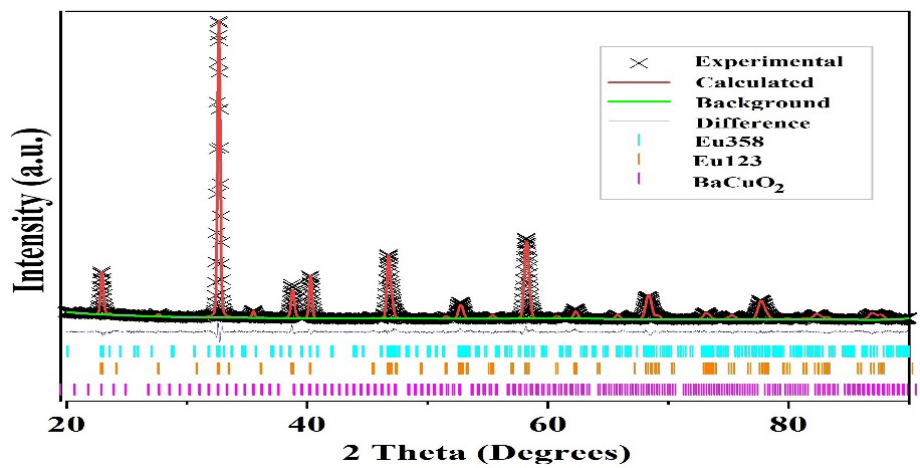

The corresponding atomic positions (*x, y, z*) and atom occupation in the unitary cell for Eu358 for the main phase as well as Eu123 and $BaCuO_2$ secondary phases respectively, are given in Tables 2, 3 and 4.

Table 1. Phase content, structural and reliability parameters, using the Rietveld refinement method.

Phase	Phase content W (%)	Lattice parameters (Å)			Cell Volume (Å^3)	Reliability Parameters	
		a	*b*	*c*		χ^2	Rf(%)
Eu358	73.08	3.889(2)	3.888(1)	30.934(1)	467.89	1.926	0.0608
Eu123	26.51	3.888(1)	3.888(1)	11.607(7)	175.48		
$BaCuO_2$	0.41	18.227(1)	18.227(1)	18.227(1)	6055.61		

Revista EIA https://doi.org/10.24050/reia.v21i42.1785

Table 2. The refinement of atomic positions and occupancy of atoms in the $EuBa_2Cu_3O_{6.4}$ (Eu123) phase.

Atom	*x*	*y*	*z*	Occ	U
Eu(1)	0.5000	0.5000	0.5000	1.0000	0.059
Ba(1)	0.5000	0.5000	0.8063	1.0000	0.007
Cu(1)	0.0000	0.0000	0.0000	1.0000	0.136
Cu(2)	0.0000	0.0000	0.6252	1.0000	0.013
O(1)	0.0000	0.0000	0.8231	1.0000	0.000
O(2)	0.0000	0.5000	0.6014	1.0000	0.000
O(3)	0.0000	0.5000	0.0000	1.0000	0.064

Table 3. The refinement of atomic positions and occupancy of atoms in the $Eu_3Ba_5Cu_8O_{18-\Delta}$ (Eu358) phase

Atoms	*x*	*y*	*z*	Occ	U
Eu(1)	0.5000	0.5000	1.0000	1.0000	0.025
Eu(2)	0.5000	0.5000	0.3750	1.0000	0.025
Eu(3)	0.5000	0.5000	0.5000	1.0000	0.025
Ba(1)	0.5000	0.5000	0.1250	1.0000	0.025
Ba(2)	0.5000	0.5000	0.2500	1.0000	0.025
Ba(3)	0.5000	0.5000	0.6250	1.0000	0.025
Ba(4)	0.5000	0.5000	0.7500	1.0000	0.025
Ba(5)	0.5000	0.5000	0.8750	1.0000	0.025
Cu(1)	0.0000	0.0000	0.0625	1.0000	0.025
Cu(2)	0.0000	0.0000	0.1875	1.0000	0.025
Cu(3)	0.0000	0.0000	0.3125	1.0000	0.025
Cu(4)	0.0000	0.0000	0.4375	1.0000	0.025
Cu(5)	0.0000	0.0000	0.5625	1.0000	0.025
Cu(6)	0.0000	0.0000	0.6875	1.0000	0.025
Cu(7)	0.0000	0.0000	0.8125	1.0000	0.025
Cu(8)	0.0000	0.0000	0.9375	1.0000	0.025
O(1)	0.0000	0.5000	0.0625	1.0000	0.025
O(2)	0.5000	0.0000	0.0625	1.0000	0.025
O(3)	0.0000	0.0000	0.1250	1.0000	0.025
O(4)	0.0000	0.5000	0.1875	1.0000	0.025
O(5)	0.0000	0.0000	0.2500	1.0000	0.025
O(6)	0.0000	0.5000	0.3125	1.0000	0.025
O(7)	0.5000	0.0000	0.3125	1.0000	0.025
O(8)	0.0000	0.5000	0.4375	1.0000	0.025

Table 3. The refinement of atomic positions and occupancy of atoms in the $Eu_3Ba_5Cu_8O_{18-\Delta}$ (Eu358) phase

Atoms	*x*	*y*	*z*	Occ	U
O(9)	0.5000	0.0000	0.4375	1.0000	0.025
O(10)	0.0000	0.5000	0.5625	1.0000	0.025
O(11)	0.5000	0.0000	0.5625	1.0000	0.025
O(12)	0.0000	0.0000	0.6250	1.0000	0.025
O(13)	0.0000	0.5000	0.6875	1.0000	0.025
O(14)	0.0000	0.0000	0.7500	1.0000	0.025
O(15)	0.0000	0.5000	0.8125	1.0000	0.025
O(16)	0.0000	0.0000	0.8750	1.0000	0.025
O(17)	0.0000	0.5000	0.9375	1.0000	0.025
O(18)	0.5000	0.0000	0.9375	1.0000	0.025

The crystalline structures for Eu358, Eu123 and $BaCuO_2$ phases were build using VESTA software (Momma et al., 2008). Phase Eu358, formed by five CuO_2 planes and three CuO chains labeled planes I to V and chains I to III, as can be observed in Fig. 4a. This structure is typical for superconductor materials, where the planes allow charge carriers transfer, and the chains act as a charge bank (Gaona et al., 2020), Landínez, et al., 2012).

Table 4. The refinement of atomic positions and occupancy of atoms in the $BaCuO_2$ phase.

Atom	*x*	*y*	*z*	Occ	U
Ba(1)	0.0000	0.1490	0.3110	1.0000	1.000
Ba(2)	0.3620	0.3620	0.0000	1.0000	1.000
Ba(3)	0.1690	0.1690	0.0000	1.0000	1.000
Ba(4)	0.0000	0.0000	0.0000	1.0000	1.000
Cu(1)	0.2500	0.1440	0.3560	1.0000	1.000
Cu(2)	0.1350	0.0000	0.1350	1.0000	1.000
Cu(3)	0.2090	0.0000	0.0000	1.0000	1.000
Cu(4)	0.4130	0.0000	0.0000	0.5000	1.000

Revista EIA https://doi.org/10.24050/reia.v21i42.1785

Table 4. The refinement of atomic positions and occupancy of atoms in the $BaCuO_2$ phase.

Atom	*x*	*y*	*z*	Occ	U
O(1)	0.0720	0.0720	0.1790	1.0000	1.000
O(2)	0.1450	0.1450	0.3350	1.0000	1.000
O(3)	0.2750	0.2750	0.0820	1.0000	1.000
O(4)	0.2500	0.0000	0.5000	1.0000	1.000
O(5)	0.3140	0.0000	0.0000	1.0000	1.000
O(6)	0.0000	0.0990	0.4350	0.2500	1.000

The unitary cell (see Fig. 4b) is formed by Eu1 cation, located between the material cells, while Eu2 and Eu3 cations are located between the Cu3-O and Cu5-O planes and separated by a 7.75Å distance. Ba1 and Ba2 cations are located between Cu1-O and Cu3-O planes, separated by a distance of 7.75 Å. On the other hand, Ba3, Ba4 and Ba5 cations are located between Cu5-O and Cu8-O planes, separated by a distance of 11.62 Å. Cu2-O chain is located between Cu1-O and Cu3-O planes. Cu6-O and Cu7-O chains are found along crystallographic b axis between Cu5-O and Cu8-O planes. Cu1-O, Cu3-O, Cu5-O, and Cu8-O planes are in tetrahedral coordination with oxygen atoms, and Cu4-O plane is located between Eu2 and Eu3 cations.

The interatomic distances between Cu and O atoms from CuO chains are located at 1.93 Å, between Cu-Cu atoms located at 3.86 Å in *c-b* plane as illustrated in Fig. 4c. The crystalline structure representation for Eu358 structure in *b-a* plane with its inclination angles and interatomic distances are exemplified in Fig 4.

Figura 4. a) Crystal structure of superconductor $Eu_3Ba_5Cu_8O_{18-\delta}$ (Eu358) with five CuO_2 planes I to V and three CuO chains I to III constructed from the refined XRD data using VESTA software. **b)** Unit cells with identified Eu, Ba, Cu y O atoms (Color Figure online). **c)** Representation of CuO chains view along the *a*-axis (*c*-*b* plane). The angle and atomic distances are exemplified in **d)** view along the *c*-axis (*b*-*a* plane).

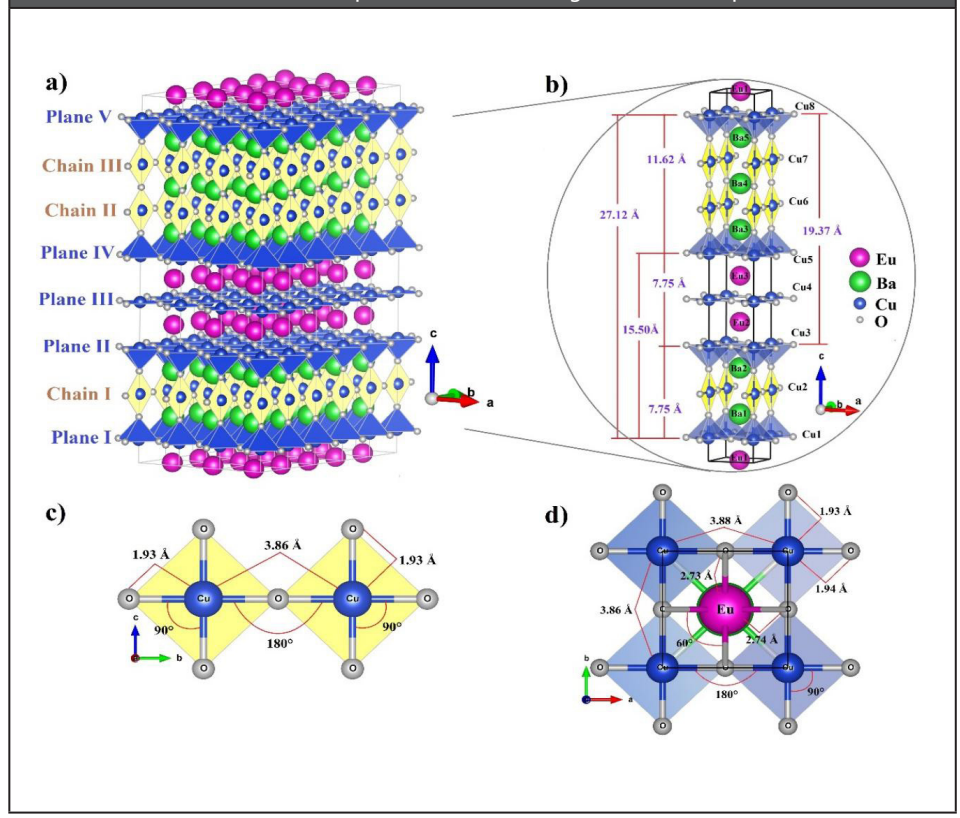

The structure for Eu123 phase is shown in Fig. 5a. In plane *c*-*b*, the Eu1 atom can be found between Cu2-O and Cu3-O planes separated by a distance of 2.90 Å, Ba1 cation is located between Cu1-O and Cu2-O planes at a distance of 4.35 Å and Ba2 cation is located between Cu3-O and Cu4-O planes, separated by y a distance of 4.35 Å. Cu1-O and Cu4-O planes can be found in octahedral coordination with oxygen atoms, and Cu2-O and Cu3-O planes are in tetrahedral coordination with oxygen atoms, as seen in the unitary cell if Fig. 5b. The angles and interatomic distances for the hexahedrons in the *c*-*b* planes and the crystalline structure of Eu123 phase, as seen from *b*-*a* plane are visualized in Figs. 5c and 5d respectively.

Revista EIA https://doi.org/10.24050/reia.v21i42.1785

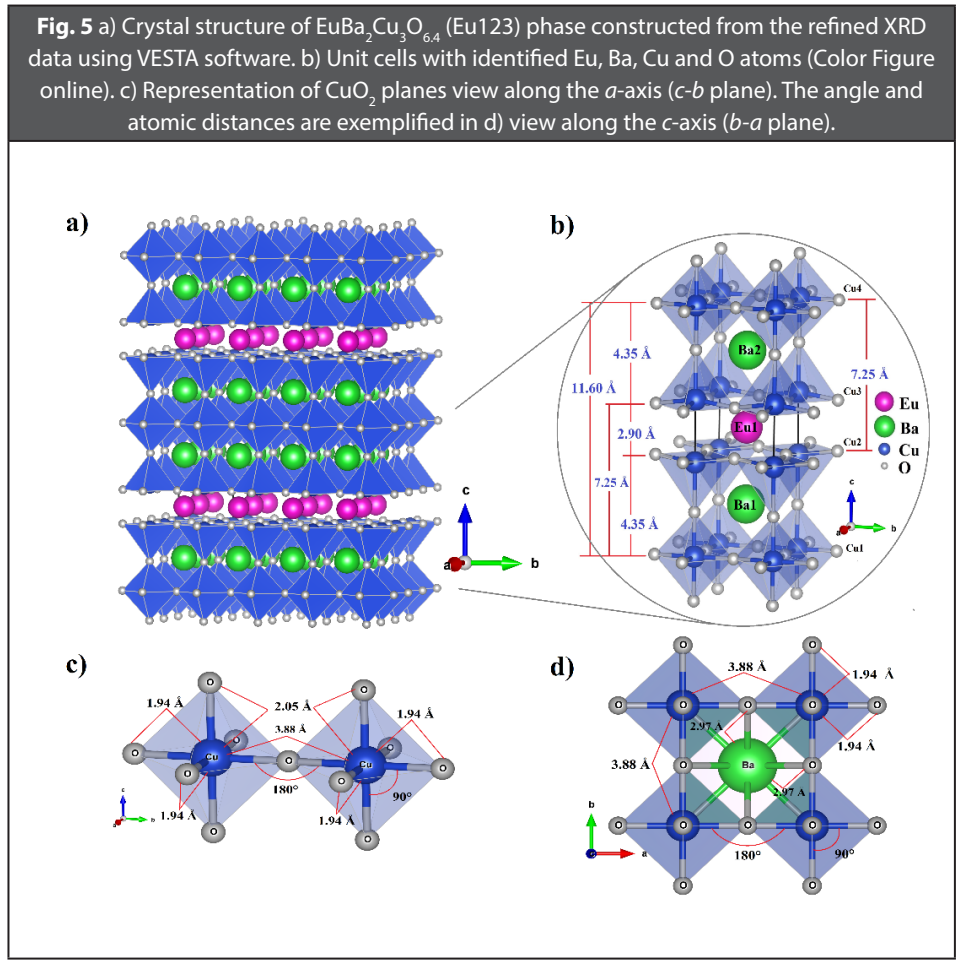

Fig. 5 a) Crystal structure of $EuBa_2Cu_3O_{6.4}$ (Eu123) phase constructed from the refined XRD data using VESTA software. b) Unit cells with identified Eu, Ba, Cu and O atoms (Color Figure online). c) Representation of CuO_2 planes view along the *a*-axis (*c*-*b* plane). The angle and atomic distances are exemplified in d) view along the *c*-axis (*b*-*a* plane).

Unitary cell for $BaCuO_2$ phase is illustrated in Fig. 6a. Ba atoms are united to O anions and Cu cations are in tetrahedral coordination with the oxygen atoms, and their angles and interatomic distances are visualized in Fig. 6b.

Fig. 6 a) Unit cells of $BaCuO_2$ phase constructed from the refined XRD data using VESTA software. The angle and atomic distances are exemplified in b) view along the *a*-axis (*c*-*b* plane)

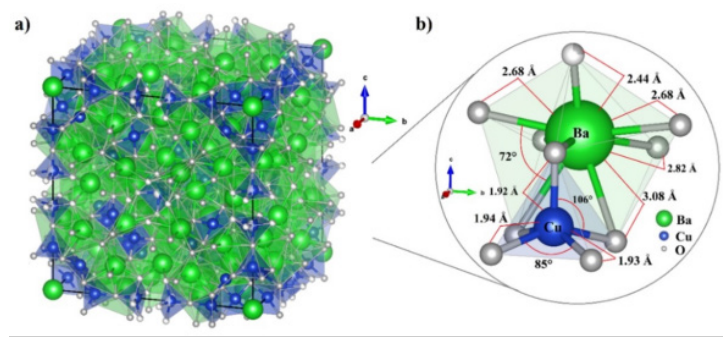

3.2 Morphological Analysis

Fig. 7 shows images for undoped $Eu_3Ba_5Cu_8O_{18-\delta}$ and $Eu_3Ba_5Cu_8O_{18-\delta}$ doped with 0.1% OG for secondary electron configurations, with 15 KX augment. $Eu_3Ba_5Cu_8O_{18-\delta}$ image (see Fig. 7a) reveals the formation of aggregates with non-uniform and non-homogeneous grains which fused together forming bigger grains, with evident necks and porosities. On the other hand, Fig. 7c shows the $Eu_3Ba_5Cu_8O_{18-\delta}$ doped with 0.1% OG where a random grain distribution was formed, with different shapes, better connections at the edges and higher homogeneity. The porosity degree decreases due to OG inclusion in the grains, which in turn increases interconnection between superconductor grains, thus facilitating electric current transport and augmenting density (Sahoo et al., 2020)).

Revista EIA https://doi.org/10.24050/reia.v21i42.1785

Fig. 7. SEM micrographs with magnification of 15 KX and analysis of the mean grain size of **a)**, **b)** $Eu_3Ba_5Cu_8O_{18-\delta}$ undoped and **c), d)** $Eu_3Ba_5Cu_8O_{18-\delta}$ doped with 0.1% graphene oxide.

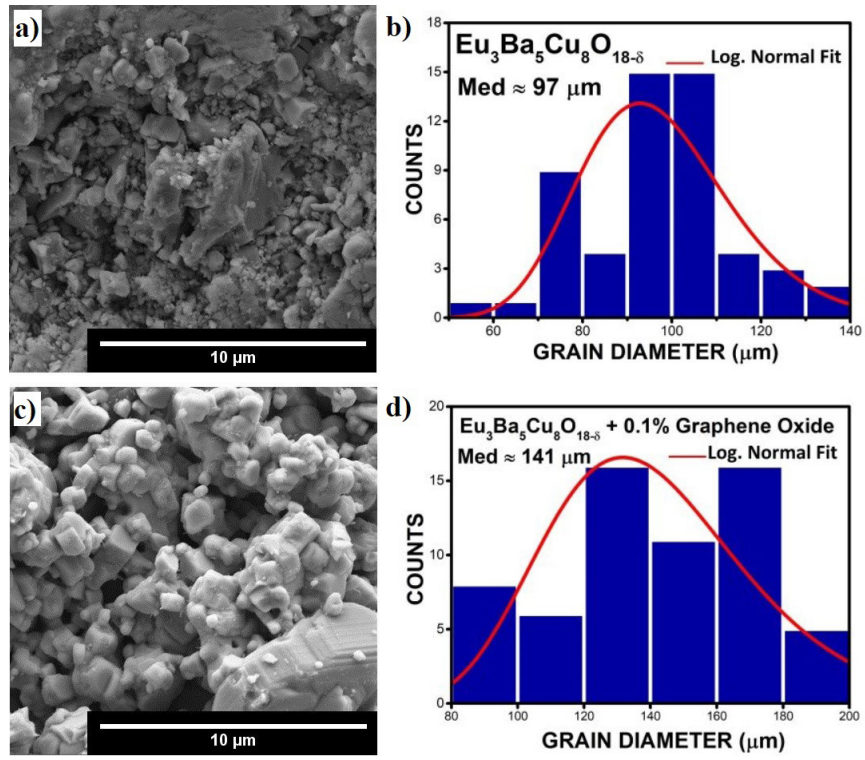

A bigger number for grain limits implies a higher amount of weak bonds, hence lesser dimensional effects over transport properties (Slimani et al., 2018)). OG doping does not change the compound's structure for $YBa_2Cu_3O_{7\delta}$ (YBCO) system, nor it changes Cu (1), Cu (2) and oxygen occupations, but increases transition temperature (T_c) and critical current density (Dadras et al., 2018). By using ImageJ software (Schneider et al., 2012), the mean size for grains in the micrographies was estimated, using a log-normal distribution adjustment with a (continuous red line Figs. 7b and 7d), which revealed a mean size of 97µm for the undoped $Eu_3Ba_5Cu_8O_{18-\delta}$ sample (see Fig. 7b) y »141 µm for $Eu_3Ba_5Cu_8O_{18-\delta}$ sample with 0.1% OG doping (see Fig. 7d). Additionally, it was demonstrated the OG does not enter the structure, but produces a betterment in weak bonds between the Eu358 grins, since the OG particles occupy the small spaces between superconductors (Sahoo et al., 2020).

Sample composition was examined by means of a semi-quantitative analysis of EDX spectra, along with atomic weight percentages for each one of the chemical element which form the material, as seen in Fig. 8 and detailed in Table 5. From the results, it can be concluded that the samples lack impurities based on other atoms, but only the expected ones from the used oxide precursors.

Figura 8. EDX spectrum obtained for the superconductor **a)** undoped **b)** doped with 0.1% graphene oxide.

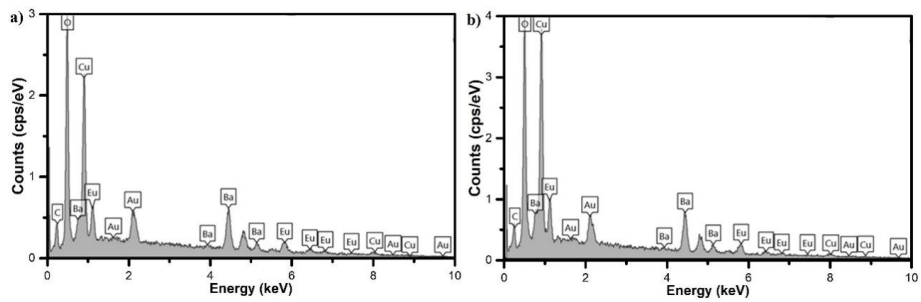

Table 5. Weight and atomic percentages of each atom in the $Eu_3Ba_5Cu_8O_{18-\delta}$ material undoped and doped with 0.1% graphene oxide obtained from EDX spectrum.

Sample	Percentage values (%)	Eu	Ba	Cu	O	C	Total
$Eu_3Ba_5Cu_8O_{18-\delta}$ undoped	Weight	29.78	29.35	18.85	16.83	5.18	100
	Atomic	8.95	9.76	13.55	48.03	19.71	100
$Eu_3Ba_5Cu_8O_{18-\delta}$ doped with 0.1% GO	Weight	32.69	25.93	21.46	15.34	4.59	100
	Atomic	10.33	9.07	16.22	46.03	18.35	100

Revista EIA https://doi.org/10.24050/reia.v21i42.1785

4. Conclusions

The superconductor material $Eu_3Ba_5Cu_8O_{18-\delta}$ was successfully synthesized through solid state reaction method, achieving 73% main superconductor phase with an orthorhombic structure and space group *Pmm2* (25). Structural analysis showed that doping with 0.1% graphene oxide lead to minority phase of $EuBa_4Cu_3O_9$ (Eu143), with a cubic structure and space group *P23* (195). Crystal size varies from 35.9 nm for undoped $Eu_3Ba_5Cu_8O_{18-\delta}$ samples, to 43.5 nm for 0.1% graphene oxide doping. Morphological characterization indicated that graphene doping increases grain size (141 μm), improving grain limit connections, thus promoting higher homogeneity.

5. References

Abdulrahman, M.W. y Hussain, F.I., 2019. Synthesis of Y3Ba5Cu8O18 superconductor by auto-combustion reaction. AIP Conference Proceedings, 2123(1). DOI: https://doi.org/10.1063/1.5117012

Alviz Meza, A., Kafarov, V. y Peña Ballesteros, D.Y., 2017. Study of the continuous corrosion in an oxidation environment derived from the theoretical combustion products in a refinery. Case study: ferritic steel ASTM A335 P91. Journal of Physics Conference Series, 935(1), p.012057. DOI: 10.1088/1742-6596/935/1/012057

Aliabadi, A., Farshchi, Y.A. y Akhavan, M., 2009. A new Y-based HTSC with Tc above 100 K. Physica C: Superconductivity and its applications, 469(22), pp.2012-2014. DOI: 10.1016/j.physc.2009.09.003

Delamare, M.P., Walter, H., Bringmann, B., Leenders, A. y Freyhardt, H.C., 2000. Characterization of natural and artificial low-angle boundaries in YBCO TSMG samples. Physica C: Superconductivity, 329(3), pp.160-177. DOI: 10.1016/S0921-4534(99)00454-200454-2)

Dadras, S., Dehghani, S., Davoudiniya, M. y Falahati, S., 2017. Improving superconducting properties of YBCO high temperature superconductor by Graphene Oxide doping. Materials Chemistry and Physics, 193, pp.496-500. DOI: 10.1016/j.matchemphys.2017.03.003

Debessai, M., Matsuoka, T., Hamlin, J.J., Bi, W., Meng, Y., Shimizu, K. y Schilling, J.S., 2010. Pressure-induced superconductivity in europium metal. Journal of Physics: Conference Series, 215(1), p.012034. DOI: 10.1088/1742-6596/215/1/012034

Dias, F.T., Oliveira, C.P.D., Vieira, V.D.N., Silva, D.L., Mesquita, F., Almeida, M.L.D. y Pureur, P., 2014. Magnetic irreversibility and zero resistance in granular Y358 superconductor. Journal of Physics: Conference Series, 568(2), p.022009. DOI: 10.1088/1742-6596/568/2/022009

Falahati, S., Dadras, S. y Mosqueira, J., 2019. Investigation of the magnetic and transport properties of YBa 2 Cu 3 O 7-δ high temperature superconductor doped with graphene oxide. Journal of Superconductivity and Novel Magnetism, 32, pp.3755-3760. DOI: 10.1007/s10948-019-05171-z

Gadzhimagomedov, S.K., Palchaev, D.K., Gadzhiev, M.K., Murlieva, Z.K., Rabadanov, M.K., Saypulaev, P.M. y Rabadanova, A.E., 2021. Superconducting YBCO ceramics after exposure to a plasma flow to a mixture of argon and oxygen. Journal of Physics: Conference Series, 1923(1), p.012007. DOI: 10.1088/1742-6596/1923/1/012007

Gaona, I.S., Supelano, G.I. y Vargas, C.P., 2020. Determination of critical superconducting parameters based on the study of the magnetization fluctuations for RE3Ba5Cu8O18-δ (RE= Sm, Eu, Gd, Dy and Ho) ceramic superconductor system. Ceramics International, 46(8), pp.11530-11538. DOI: 10.1016/j.ceramint.2020.01.179

Gholipour, S., Daadmehr, V., Rezakhani, A.T., Khosroabadi, H., Shahbaz Tehrani, F. y Hosseini Akbarnejad, R., 2012. Structural phase of Y358 superconductor comparison with Y123. Journal of superconductivity and novel magnetism, 25, pp.2253-2258. DOI: 10.1007/s10948-012-1611-4

Guerrero, U.F., Rivera, A.M., Cuaspud, J.A., Munevar, J. y Vargas, C.A., 2021. Synthesis of the La 3 Ba 5 Cu 8 O 18-δ and Sm 3 Ba 5 Cu 8 O 18-δ superconductors by the combustion and solid-state reaction methods. Materials Research, 24. DOI: 10.1590/1980-5373-MR-2020-0366

Hor, P.H., Gao, L., Meng, R.L., Huang, Z.J., Wang, Y.Q., Forster, K. y Torng, C.J., 1987. High-pressure study of the new Y-Ba-Cu-O superconducting compound system. Physical review letters, 58(9), p.911. DOI: 10.1103/PhysRevLett.58.911

JG, B., 1986. Possible highT_c super-conductivity in the Ba-La-Cu-O system. Z Physik B, 64, pp.189-193. DOI: 10.1007/BF01303701

Kamarudin, A.N., Awang Kechik, M.M., Abdullah, S.N., Baqiah, H., Chen, S.K., Abdul Karim, M.K. y Talib, Z.A., 2022. Effect of Graphene Nanoparticles Addition on Superconductivity of YBa2Cu3O7∼ δ Synthesized via the Thermal Treatment Method. Coatings, 12(1), p.91. DOI: 10.3390/coatings12010091

Kraus, W. y Nolze, G., 1996. POWDER CELL–a program for the representation and manipulation of crystal structures and calculation of the resulting X-ray powder patterns. Journal of applied Crystallography, 29(3), pp.301-303. DOI: 10.1107/S0021889895014920

Kumar, N., Das, S., Bernhard, C. y Varma, G.D., 2013. Effect of graphene oxide doping on superconducting properties of bulk MgB2. Superconductor Science and Technology, 26(9), p.095008. DOI: 10.1088/0953-2048/26/9/095008

Landínez Téllez, D.A., Cabrera Baez, M. y Roa-Rojas, J., 2012. Structure and conductivity fluctuations of the Y 3 Ba 5 Cu 8 O 18 superconductor. Modern Physics Letters B, 26(11), 1250067. DOI: 10.1142/S0217984912500674

Momma, K. y Izumi, F., 2008. VESTA: a three-dimensional visualization system for electronic and structural analysis. Journal of Applied crystallography, 41(3), pp.653-658. DOI: 10.1107/S0021889808012016

Parra Vargas, C.A., Canaría-Camargo, C.C., Roa-Rojas, J. y Albino-Aguiar, J., 2021. Análisis estructural del sistema superconductor RE3Ba5Cu8O18 (RE= Dy, Gd, Ho, Sm, Y, Yb). DOI: 10.18257/raccefyn.1163

Parra-Borda, J.A., Rojas-Cruz, F.G., Cruz-Pacheco, A.F., Segura-Peña, S. y Vargas, C.P., 2017. Structural and magnetic analysis of the Pr1. 5Eu1. 5Ba5Cu8O18 system. Journal of Physics: Conference Series, 935(1), p.012005. DOI: 10.1088/1742-6596/935/1/012005

Pavan Kumar Naik, S., Santosh, M. y Swarup Raju, P.M., 2018. Structural and thermal validations of Y 3 Ba 5 Cu 8 O 18 composites synthesized via citrate sol-gel spontaneous combustion method. Journal of Superconductivity and Novel Magnetism, 31, pp.1279-1286. DOI: 10.1007/s10948-017-4306-z

Rekaby, M., Roumié, M., Abou-Aly, A.I., Awad, R. y Yousry, M., 2014. Magnetoresistance study of Y 3 Ba 5 Cu 8 O 18 superconducting phase substituted by Nd 3+ and Ca 2+ ions. Journal of Superconductivity and Novel Magnetism, 27, pp.2385-2395. DOI: 10.1007/s10948-014-2572-6

Sahoo, B., Singh, A.K. y Behera, D., 2020. Graphene oxide modified superconducting and elastic parameters of YBCO superconductor. Materials Chemistry and Physics, 240, 122252. DOI: 10.1016/j.matchemphys.2019.122252

Schneider, C.A., Rasband, W.S. y Eliceiri, K.W., 2012. NIH Image to ImageJ: 25 years of image analysis. Nature methods, 9(7), pp.671-675. DOI: 10.1038/nmeth.2089

Shoushtari, M.Z., Heidarzadeh, G. y Ghahfarokhi, S.M., 2018. An Investigation of Y 3 Ba 5 Cu 8 O 18 Doping with Ag Nanoparticles and Its Application as Superconductor. Journal of Superconductivity and Novel Magnetism, 31, pp.3475-3483. DOI: 10.1007/s10948-018-4581-3

Slimani, Y., Hannachi, E., Azzouz, F.B. y Salem, M.B., 2018. Impact of planetary ball milling parameters on the microstructure and pinning properties of polycrystalline superconductor Y3Ba5Cu8Oy. Cryogenics, 92, pp.5-12. DOI: 10.1016/j.cryogenics.2018.03.010

Sahoo, B., Karmakar, S. y Behera, D., 2019. Improvement of critical parameters of YBCO superconductor by addition of graphene oxide. AIP Conference Proceedings, 2162(1). DOI: 10.1063/1.5130270

Suan, M.S.M., Johan, M.R. y Siang, T.C., 2012. Synthesis of Y3Ba5Cu8O18 superconductor powder by auto-combustion reaction: effects of citrate–nitrate ratio. Physica C: Superconductivity, 480, pp.75-78. DOI: 10.1016/j.physc.2012.05.006

Supelano, G.I., Santos, A.S. y Vargas, C.P., 2014. Magnetic fluctuations on TR3Ba5Cu8Oδ (TR= Ho, Y and Yb) superconducting system. Physica B: Condensed Matter, 455, pp.79-81. DOI: 10.1016/j.physb.2014.07.050

Tavana, A. y Akhavan, M., 2010. How T c can go above 100 K in the YBCO family. The European Physical Journal B, 73, pp.79-83. DOI: 10.1140/epjb/e2009-00396-7

Toby, B.H., 2001. EXPGUI, a graphical user interface for GSAS. Journal of applied crystallography, 34(2), pp.210-213. DOI: 10.1107/S0021889801002242

Topal, U., Akdogan, M. y Ozkan, H., 2011. Electrical and structural properties of RE 3 Ba 5 Cu 8 O 18 (RE= Y, Sm and Nd) superconductors. Journal of superconductivity and novel magnetism, 24, pp.2099-2102. DOI: 10.1007/s10948-011-1176-7

Topal, U. y Akdogan, M., 2012. The Role of Oxygenation on Superconducting Properties of RE 3 Ba 5 Cu 8 O 18 (RE= Y, Sm and Nd) Compounds. Journal of superconductivity and novel magnetism, 25, pp.239-244. DOI: 10.1007/s10948-011-1285-3

Udomsamuthirun, P., Kruaehong, T., Nilkamjon, T. y Ratreng, S., 2010. The new superconductors of YBaCuO materials. Journal of superconductivity and novel magnetism, 23, pp.1377-1380. DOI: 10.1007/s10948-010-0786-9

Walter, H., Delamare, M.P., Bringmann, B., Leenders, A. y Freyhardt, H.C., 2000. Melt-textured YBaCuO with high trapped fields up to 1.3 T at 77 K. Journal of Materials Research, 15(6), pp.1231-1234. DOI: 10.1557/JMR.2000.0175

Wei, K., Ing, K., Hamdan, M.S., Radiman, S. y Abd-Shukor, R., 2018. AC Susceptibility and superconducting properties of graphene added YBa 2 Cu 3 O 7− d. Journal of Superconductivity and Novel Magnetism, 31, pp.2699-2703. DOI: 10.1007/s10948-017-4536-0

Zhu, Y., Murali, S., Cai, W., Li, X., Suk, J.W., Potts, J.R. y Ruoff, R.S., 2010. Graphene and graphene oxide: synthesis, properties, and applications. Advanced materials, 22(35), pp.3906-3924. DOI: 10.1002/adma.201001068